*Desalination and Water Treatment*
www.deswater.com

doi: 10.1080/19443994.2014.972731

56 (2015) 2618–2630
December

Taylor & Francis
Taylor & Francis Group

# A research on water desalination using membrane distillation

Khaled Nakoa*, Abhijit Date, Aliakbar Akbarzadeh

*Aerospace, Manufacturing and Mechanical Engineering, RMIT University, Victoria, Australia, Tel. +61 3 9925 6224; email: s3302136@student.rmit.edu.au (K. Nakoa), Tel. +61 3 9925 0612; email: abhijit.date@rmit.edu.au (A. Date), Tel. +61 3 9925 6079; email: aliakbar.akbarzadeh@rmit.edu.au (A. Akbarzadeh)*

Received 22 November 2013; Accepted 13 June 2014

---

## ABSTRACT

This research work aimed to investigate the performance of direct contact membrane distillation (MD) unit under different conditions. A mathematical model was developed to evaluate the experimental values of the membrane water mass flux, heat transfer coefficients, the membrane/liquid interface temperatures, the temperature polarization coefficient (TPC) and the evaporation efficiency. This model was solved numerically using MATLAB® software, and its results were used to predict the actual performance of the membrane unit. The MD coefficient was evaluated from the computer model data and was subsequently used to estimate water fluxes. Experimental tests were performed using 0.0572 $m^2$ of poly-tetra-fluoroethylene membrane manufactured by membrane solution (85% porosity, 45-m thickness, 0.22-m nominal pore size). Feed solutions were aqueous NaCl solutions with 1,000–200,000 mg/L (0.1–20%) in concentration, its temperatures were 40–80˚C and feed flow rate was 2 l/min. The temperature and flow rate of permeate water was fixed at 20˚C and 3 l/min, respectively. The experimental observation showed that the vapour mass flux through the membrane pores increased with feed temperature, but decreased with feed concentration. It was found that the predicted mass fluxes agreed reasonably with the experimental data, except at a high feed concentration. The temperature polarization coefficients increased with concentration and decreased with increasing temperature. The membrane heat transfer rates and the permeate flux have been discussed in this paper.

*Keywords:* Membrane distillation; Water desalination; Membrane distillation coefficient; Permeate mass flux

---

## 1. Introduction

Since 1950, global demand for freshwater has approximately doubled every 15 years. About 450 million people in 29 countries face severe water shortages; about 20% more water than now available will be needed to feed the additional 3 billion people by 2025 [1]. This growth has reached a point where today existing freshwater resources are under great stress, and it has become both more difficult and more expensive to develop new freshwater resources. One especially relevant issue is that a large proportion of the world's population (approximately 70%) dwells in coastal

---

*Corresponding author.

*Presented at the 4th Maghreb Conference on Desalination and Water Treatment (CMTDE 2013)*
*15–18 December 2013, Hammamet, Tunisia*

1944-3994/1944-3986 © 2014 Balaban Desalination Publications. All rights reserved.

zones [2]. Furthermore, the World Health Organization reported that 20% of the world population has inadequate drinkable water. Even though the two-third of the planet is covered with water, 99.3% of this water either has high salinity or not accessible (ice caps) [3]. The current mean population density at coastlines is almost 100 hab/km$^2$, and it is over 2.5 times the global average and embraces 45% of the global population [4]. Many of these coastal regions rely on underground aquifers for a substantial portion of their freshwater supply. In particular, if an aquifer is overdrawn, it can be contaminated by an influx of sea water or salts and, therefore, requires a treatment or purification. So the combined effects of increasing freshwater demand, population growth and sea water intrusion into coastal aquifers are stimulating the demand for desalination. Desalination is a process of removing salts and other minerals from a saline water solution producing freshwater, which is suitable for human consumption, agriculture and industrial use. Generally, the desalination system usually consists of three main parts; water source, desalination unit and energy source which are playing the key role in evaluating the desalination plant performance. Water source can be brackish water or sea water. Furthermore, the desalination systems can be classified into three categories; thermal process that uses phase change process such as multi-effect desalination and multi-stage flash (MSF); membrane process that uses a certain membrane without liquid phase change such as reverse osmosis (RO) and electrodialysis. The third one is the hybrid system that involves two processes, phase change and membrane technology such as thermal membrane distillation (MD). The membrane is defined as a thin barrier between two fluids that allows particles or chemicals to pass through but not others. Furthermore, hydrophobic microporous membrane is the most preferable membrane type that is used with MD. MD process has hot and cold streams at both sides of the membrane, and it can produce very high pure water from saline or waste water. The vapour–liquid interface forms at the pore entrance on the hot feed side; then, the volatile components such as vapour diffuse through the pore and condense at the cold permeate side. The driving force of the vapour is the hydrostatic pressure difference resulted from the temperature difference between hot and cold membrane surfaces.

The invention of membrane was in 1963 by Bodell. In 1967, first paper about MD was published by Findley [5]. The death phase of MD research occurred from 1970 to 1980 as indicated by no reported study can be found [6]. In the 1980s, a new membrane with better characteristics has become available [7]. The number of researchers and intensive works performed on MD has been increased noticeably from late 1990s to 2005, resulted in major advancement and present different MD configuration [7]. Furthermore, the capability to utilize the low-grade heat source such as waste heat, geothermal or solar energy with MD makes it more promising future technology.

Some MD benefits are as follows:

- It can produce freshwater at low temperature which is provided by low-grade heat source such as solar energy, waste heat and geothermal.
- High salt rejection can be achieved.
- It can work near to saturated concentration.
- It works at low hydrostatic pressure.
- Pre-treatment is cost-effective compared to RO process.
- Less sensitive to feed characteristics (PH, TDS, etc.)

Even though MD has some advantages over other desalination technology, using MD commercially still need to be more investigated, and it should be implemented in the industrial sector with large-scale and long-term application. MD can be commercialized if these requirements are satisfied:

- High liquid entry pressure.
- High permeability.
- Low thermal conductivity.

Commercially, there are four main membrane types that can be used with MD available in the market. They are polypropylene, poly-vinylidene fluoride, PTFE, and polyethylene which are available in tubular, capillary, and flat-sheet forms.

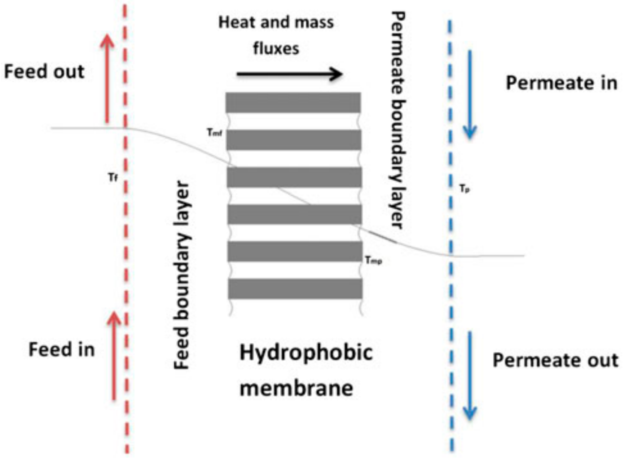

Fig. 1. Heat boundary layers at two sides of the membrane.

MD has different configurations which are defined as to the method of recovering the vapour after it has immigrated through membrane pores. The oldest and common one is the direct contact membrane distillation (DCMD) where liquid phases are in direct contact with both surfaces of the membrane as shown in Fig. 1. The alternative methods are air gap membrane distillation, vacuum membrane distillation and sweeping gas membrane distillation [5].

Recently, researchers investigated several characteristics of membranes such as porosity or pore size, thickness and material. The porosity is the ratio between the pore size and the solid size of the membrane. It varies between 30 and 80%, and it has a significant effect on membrane mass flux or transmembrane parameter [7]. Also, the pore size which is ranging between 100 nm and 1 μm has the same effect on mass flux; as it increases, the transmembrane increases. Another character is the pore distribution in the membrane surface, but its effect on MD flux has not been sufficiently investigated. Finally, the effect of membrane material and thickness are still under investigation. Membranes may produce more fresh water by choosing appropriate material with low surface energy, pore size and high hydrophobicity [5]. In general, membrane area does not have a significant effect on the flux rate, but it lowers the specific energy consumption substantially [8]. Another aspect is that the MD mass flux increases with feed mass-flow velocity and reaches asymptotic level at higher rates. The permeate flux increases with feed temperature, temperature difference and permeate-side flow velocity [7]. They affect the heat transfer coefficient which is consequently affecting the mass flux.

Furthermore, solar energy can be used as an energy source, and it can be combined with desalination technology either by producing thermal resource (solar thermal) for water heating or by generating electricity (photovoltaic) to drive the membrane process. Some researchers reported that the thermal and electrical energy consumption was 55.6 kWh/m$^3$. Also, a mass flux of 17 l/d/m$^2$ of collector area was determined and comparable to that reported for solar MSF and ME plants [3]. Furthermore, one of the most common sources of thermal energy is the solar pond where heat can be extracted from the storage zone at the bottom layer of the pond. The annual energy efficiency of useful heat that can be delivered to a desalination plant by solar pond is about 10–15% [3].

## 2. Theoretical approach

In MD, the driving force for water vapour transfer through the membrane pores is the temperature difference between the feed/membrane interface temperature $(T_1)$ and the permeate/membrane interface temperature $(T_2)$. This generates a different vapour pressure at both membrane sides and forces the vapour molecules to travel through the membrane pores.

### 2.1. Flow mechanisms

There are three basic mechanisms of mass flow inside the membrane wall, which are Knudsen diffusion, Poiseuille flow and molecular diffusion. In Knudsen diffusion, the pore size is too small, and the collision between molecules can be neglected. Furthermore, the collision between sphere molecules and the internal walls of the membrane is the dominant mass transport form. Molecular diffusion occurs if the pore size is big comparing to the mean free path of molecules, and they move corresponding to each other. The flow is considered Poiseuille (viscous flow) if the molecules act as continuous fluid inside the membrane pores. In general, different mechanisms occur simultaneously (Knudsen, Poiseuille and molecular diffusion) inside the membrane if the pore size is less than 0.5 m [9].

### 2.2. Knudsen number

It is a governing quantity of the flow mechanism inside the membrane pores which is the ratio between the mean free path of the transported molecules and the pore size of the membrane. For an instant, the mean free path for water vapour at 50˚C under atmospheric pressure is approximately 0.14 m [5]. The Knudsen number $Kn$ is defined in the following equation and is used to determine the dominating mechanism of mass transfer inside the pore:

$$kn = \frac{S}{d} \tag{1}$$

$S$ is the mean free path of the transferred gas molecule, and $d$ is the mean pore diameter of the membrane.

$S$ is calculated from the following:

$$\frac{k_B T}{\sqrt{2}\pi P d_e^2} \tag{2}$$

$k_B$, $T$, and $P$ are Boltzmann constant $(1.380622 \times 10^{-23}\, J/K)$, absolute temperature and average pressure inside the membrane pores, respectively. $d_e$

is the collision diameter of the water vapour and air which is $2.64 \times 10^{-10}$ and $3.66 \times 10^{-10}$ m, respectively [9].

The pore sizes of the most membranes are in the range of 0.2–1.0 m. The mean free path of water vapour is 0.11 m at feed temperature of 60°C. Therefore, *kn* is in the range of 0.11–0.55.

The different flow mechanisms inside the membrane pores can be identified by Knudsen number *kn*:

| | |
|---|---|
| $kn < 0.01$ | Molecular diffusion |
| $0.01 < kn < 1$ | Knudsen–molecular diffusion transition mechanism |
| $kn > 1$ | Knudsen mechanism |

### 2.3. Mass flux (J)

As shown in Fig. 1, vapour in transferring from feed side of the membrane to the permeate side by pressure difference force is resulted from the temperature difference between two sides. The mass transfer may be written as a linear function of the vapour pressure difference across the membrane, given by

$$J = C_m(P_1 - P_2)\,\mathrm{kg/m^2/s} \tag{3}$$

where $J$ is the mass flux, $C_m$ is the MD coefficient, and $P_1$ and $P_2$ are the partial pressure of water vapour evaluated at the membrane surface temperatures $T_1$ and $T_2$.

$C_m$ for Knudsen flow mechanisms:

$$C_m^k = \frac{2\varepsilon r}{3\tau\delta}\left(\frac{8M}{\pi RT}\right)^{1/2} \tag{4}$$

$C_m$ for molecular diffusion:

$$C_m^D = \frac{\varepsilon}{\tau\delta}\frac{PD}{P_a}\frac{M}{RT} \tag{5}$$

$C_m$ for Knudsen–molecular diffusion transition mechanism:

$$C_m^C = \left[\frac{3}{2}\frac{\tau\delta}{\varepsilon d}\left(\frac{\pi RT}{8M}\right)^{1/2} + \frac{\tau\delta}{\varepsilon}\frac{P_a}{PD}\frac{RT}{M}\right]^{-1} \tag{6}$$

$D$ is the diffusion coefficient of the vapour in the air. $P$ is the pressure at $\bar{T}$ and can be found using Antoine equation:

$$P = \exp\left(23.238 - \frac{3{,}841}{\bar{T}\,45}\right) \tag{7}$$

($\bar{T}$) is the average membrane temperature.

### 2.4. Heat flux (q)

The heat transfer models of MD can be summarized as follows:

- Convective heat transfer from the feed side to the membrane surface boundary layer:

$$q_f = h_f(T_f - T_1) \tag{8}$$

where $q_f$ is the feed heat flux (W/m$^2$) and $h_f$ is the heat transfer coefficient (W/m$^2$ K).

- Heat flux through the membrane which includes conduction heat flux through the solid material of the membrane $k_m \frac{dt}{dx}$, and the latent heat transfer as a conviction by water vapour through the pores $JH_v$:

$$q_m = JH_v + k_m\frac{dt}{dx} \tag{9}$$

$H_v$ is the vaporization enthalpy of water evaluated at the mean temperature $\frac{T_1+T_2}{2}$, and the second term is the conduction heat loss through the membrane material.

Finally, heat is transferred through the permeate boundary layer to the permeate water by convection.

$$q_p = h_p(T_2 - T_p) \tag{10}$$

At steady state:

$$q_f = q_m = q_p \tag{11}$$

The overall heat transfer coefficient can be determined by the following:

$$U = \left[\frac{1}{h_f} + \frac{1}{\frac{k_m}{\delta_m} + \frac{JH_v}{T_1 - T_2}} + \frac{1}{h_p}\right]^{-1} \tag{12}$$

The rate of total heat transferred through the membrane is as follows:

$$q_t = U(T_f\_T_p) \tag{13}$$

The feed flow energy balance is as follows:

$$q_f = \dot{m}_f c_p (T_{f,\text{in}} - T_{f,\text{out}}) \tag{14}$$

The thermal efficiency of the membrane is as follows:

$$E_t\ (\%) = \frac{JH_v A}{Q_t} \times 100 \tag{15}$$

The thermal efficiency is the ratio between the water heat energy consumption to generate vapour and the total heat energy supplied to the system, whereas heat conduction through membrane solid is considered heat loss and it should be minimized.

To be more adequate, the efficiency should include both thermal and electrical energy (pumps); thus, gained output ratio (GOR) can define it as follows:

$$\text{GOR} = \frac{JH_v A}{E_T + E_E \times t} \tag{16}$$

To determine heat transfer coefficients of the boundary layers at both membrane sides, the average bulk temperature of feed side $\frac{T_f+T_1}{2}$, and at permeate side $\frac{T_2+T_p}{2}$ of the membrane should be used. Graetz–Leveque correlation is recommended [10]:

$$N_u = 1.86\left(R_e P_r \frac{d_h}{L}\right)^{0.33} \quad d_h = \frac{4A_c}{P_e} \tag{17}$$

This correlation can be used for laminar flow ($R_e < 2{,}100$).

In contrast, next correlation can be applied for turbulent flow ($2{,}500 < R_e < 1.25 \times 10^5$ and $0.6 < P_e < 100$).

$$N_u = 0.023\, Re^{0.8} Pr^n \tag{18}$$

where $n$ is equal to 0.4 for heating, and 0.3 for cooling [11].

The dimensionless groups, Nusselt number ($v$), Reynolds number ($R_e$) and Prandtl number ($P_r$) can be calculated straightforwardly using the available physical data of feed and permeate fluid.

At both sides of the membrane where the vapour–liquid interface takes place, there is a thermal boundary layer in which its temperature differs from the bulk stream. This difference is described as temperature polarization coefficient (TPC) or ($\lambda$).

$$\lambda = \frac{T_1 - T_2}{T_f - T_p} \tag{19}$$

The iterative method by a computer software (MATLAB©) is applied to predict $T_1$ and $T_2$. After entering the geometry and fluid properties, the software initially calculates the boundary heat transfer coefficients those to be used with next correlations. Then, it uses the values of $T_1$ and $T_2$ which are assumed equal to the bulk temperature $T_f$ and $T_p$, respectively, to determine the new values of $T_1$ and $T_2$ by a number of iterations. Eqs. (21) and (22) are used for predicting both temperatures. Once the surface temperatures $T_1$ and $T_2$ are determined, the software calculates the rest of required parameters. Please refer to the appendix A about those values.

To determine the evaporation latent heat:

$$H_v \text{ is evaluated at } T = \frac{T_1 + T_2}{2} \tag{20}$$

Finally,

$$T_1 = \frac{h_m\left(T_p + (h_f/h_p)T_f\right) + h_f T_f - JH_v}{h_m + h_f(1 + h_m/h_p)} \tag{21}$$

$$T_2 = \frac{h_m\left(T_f + (h_p/h_f)T_p\right) + h_p T_p + JH_v}{h_m + h_p(1 + h_m/h_f)} \tag{22}$$

where

$$h_m = \frac{k_m}{\delta_m} \tag{23}$$

## 3. The experiment

Experimental tests were performed using a PTFE membrane manufactured by membrane solution (85% porosity, 45-m thickness, 0.22-m nominal pore size). The main part of the used experimental set-up as shown in Fig. 2 is a plastic block (300 × 260 × 40 mm) which is divided into two symmetrical halves (Fig. 3). The membrane sheet is placed between them, and a gap of 2 mm is provided between the membrane and the block surface to allow feed and permeate water flow. The effective membrane area for the transport was 0.0572 m, and it was supported by plastic net spacer. In all experimental runs, the membrane was maintained in a horizontal position. The feed (saline

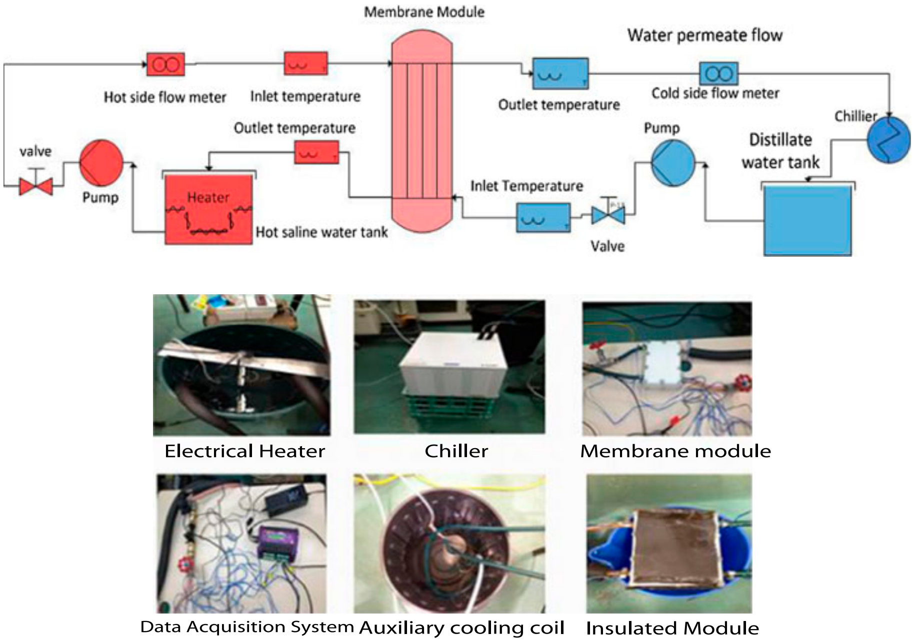

Electrical Heater Chiller Membrane module

Data Acquisition System Auxiliary cooling coil Insulated Module

Fig. 2. Experimental set-up of DCMD.

water) was heated inside a container by thermostatic heater and then pumped onto the membrane lower surface. The water at permeate side was cooled down by a water chiller in another container and then pumped onto the upper membrane surface. The recirculation of the both sides of the membrane was in counter-current directions. The temperatures of the bulk liquid phases are measured at the hot entrance ($T_{f1}$), the cold entrance ($T_{p1}$), the hot exit ($T_{f2}$) and the cold exit ($T_{p2}$), of the membrane module. These temperatures will be different from the temperatures at the hot and cold membrane sides, $T_1$ and $T_2$, respectively. In this experimental set-up, permeate water continuously collected in the distillate reservoir, and the corresponding distillate flux was measured by an electronic scale at the distillate reservoir. Furthermore, in this work, experiments were conducted with feed sodium chloride solutions of concentrations 0.1, 1, 3.7, and 20% of density. Likewise in all cases, the recirculation flow rates on both membrane surfaces were 2 l/m at feed side and 3 l/m at permeate side.

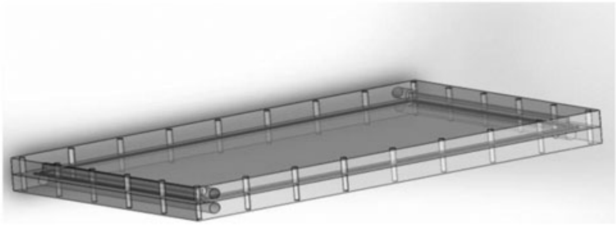

Fig. 3. The acrylic plastic block of DCMD module with two inlets and two outlets.

Different experiments were carried out for fixed temperatures in the membrane module. The feed temperature $T_{f1}$ varied from 40 to 80°C at increments of about 10°C, and the cooling water temperature $T_{p1}$ varied from 18 to 23°C.

## 4. Results and discussion

In Fig. 4, the distillate mass fluxes are presented as a function of temperature difference with different salt concentrations. These mass fluxes are the average value of at least three experiments obtained when temperatures $T_{f,\text{in}}$, $T_{f,\text{out}}$, $T_{p,\text{in}}$, and $T_{p,\text{out}}$ were recorded by connected thermocouples.

The steady-state fluxes at different salinities were also plotted against the vapour pressure differences ($P_1{-}P_2$) calculated at the membrane surface temperatures ($T_1$, $T_2$) as shown in Figs. 5a and 5b.

The slope of the straight line is the MD coefficient, $C = 0.001\ \text{kg/m}^2\ \text{s Pa}$ (see Eq. (3)). $C_m$ is a constant rely on the membrane characteristics and channel and vapour properties. Also, the coefficient $C_m$ may decrease due to the reduction of the surface area available for evaporation if the concentration polarization and fouling are existed. The value of $C_m$ obtained in this study was less than that

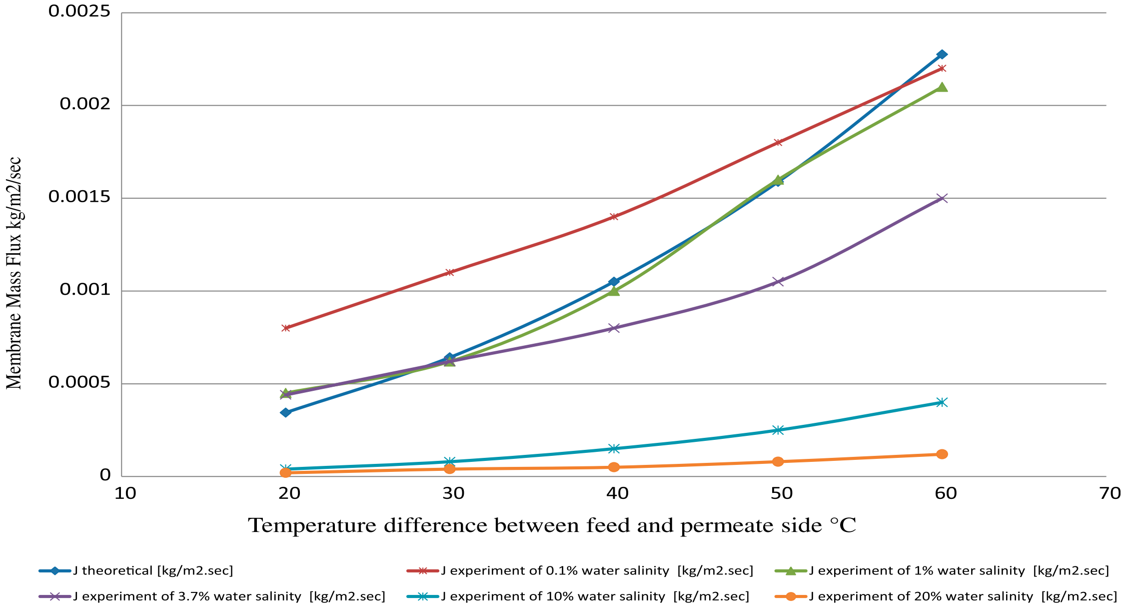

Fig. 4. Effect of water feed salinity and temperature difference on membrane mass flux.

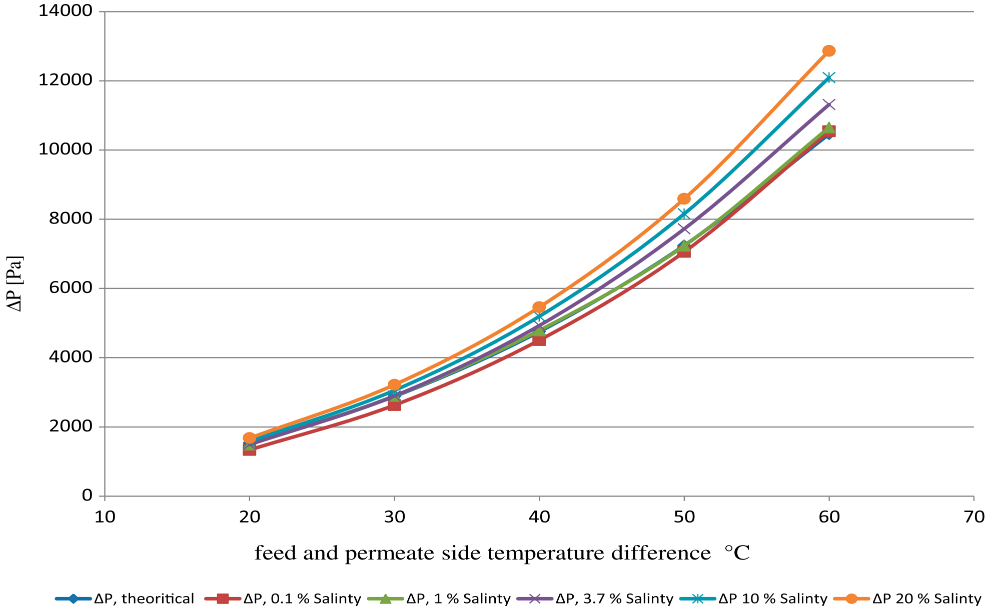

Fig. 5(a). Pressure difference variation with different salinities and temperature difference.

reported in the literature [6,8]. This is due to low water flow at both sides of the membrane. Actually, the reduction of mass flux is attributed to the fact that the addition of the salt reduces the partial vapour pressure of water according to Raoul's law (Eq. (24)) and thus reduces the driving force of mass transfer through the membrane.

$$P^s = (1 - x_i)P^v \tag{24}$$

where $x_i$ is the solute mole fraction in the bulk liquid, $P^v$ is the vapour pressure of pure water at the feed temperature in $Pa$ and $P^s$ is the partial vapour pressure of water in $Pa$ at the same temperature.

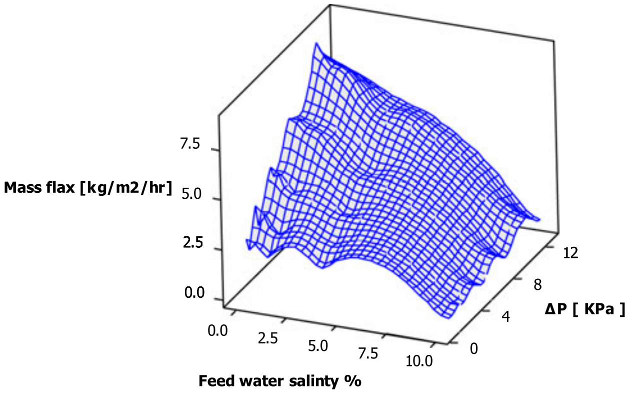

Fig. 5(b). Mass flux variation with salinity and pressure difference.

### 4.1. Effect of feed temperature

Fig. 6 compares the mass flux of distillate water and the feed stream temperature. The increase in mass flux was dependent on temperature at feed side, and the values were also in the reported range [9,12]. It was observed that the mass flux increases significantly with feed temperature especially at lower salinities. Moreover, the presence of NaCl in the feed aqueous solution will form an additional boundary layer adjacent to the membrane surface. This concentration boundary layer, together with the temperature boundary layer, further reduces the driving force. It must also be pointed out that in all experiments, the solute separation factor defined as (feed solute concentration–permeate solute concentration)/(feed solute concentration) was higher than 99% [12].

### 4.2. Effect of feed concentration

Mass flux decreased with increasing feed concentration (see Fig. 4). The decrease in vapour pressure is the main cause and plays an important role. Flux decline over time was also observed, but it was more significant at high concentration. This suggested a possible effect of both concentration and temperature polarization. The values of 0.27–0.32 TPC are shown in Fig. 7. The increase in retentate concentrations was examined and was found to be only 2–3% at 60°C (after 9 h). Accordingly, concentration polarization may be significant at high concentration, high temperature and low flow rate. In this study, low flow rate was applied; thus, the TPC was low, and consequently, the membrane mass flux was low. The values of TPC were experimentally evaluated and obtained using Eq. (19) under various conditions. It was found

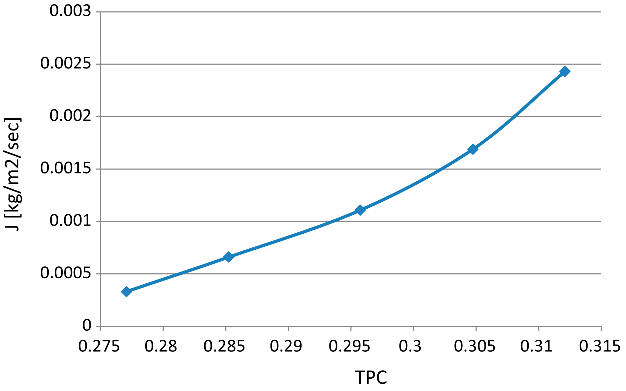

Fig. 7. Mass flux variation with TPC.

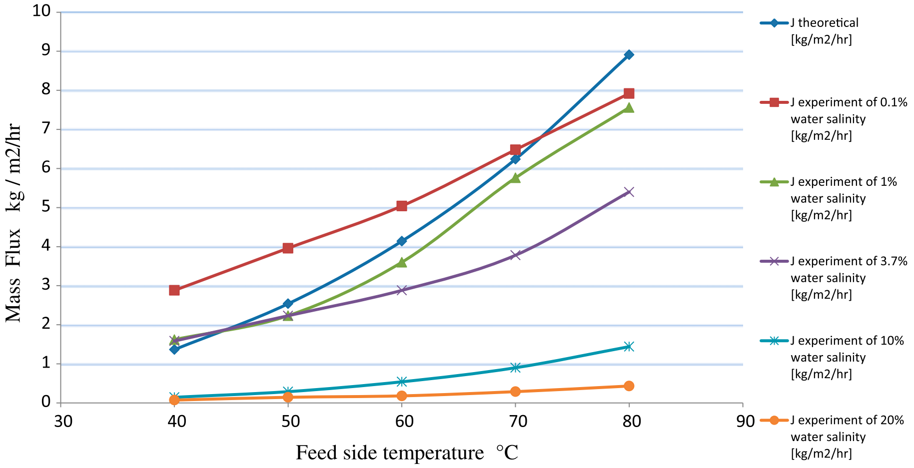

Fig. 6. Effect of feed-side water temperature on mass flux permeation.

that the TPC increases exponentially from 0.27 to 0.32. Also, Fig. 7 indicates that the increase in mass flux with TPC is quite significant at values greater than 0.29. For instant, the increase in TPC with flow rates or Reynolds number is relatively logical as the developed flow pattern within the module channel by increasing Reynolds number trends to the mixing of the fluid present at the membrane interface and in the bulk. Consequently, the temperature distribution layer adjacent the membrane surface becomes more homogeneous and attributes a positive influence to TPC. The effect is more noticeable with laminar flow as smaller increase will increase the mixing significantly. The effect is relatively smaller in transition region and becomes even minor in turbulent region as the further increase in Reynolds number does not influence the mixing substantially.

In contrast, high values of TPC are due to the high values of the boundary layers' heat transfer coefficients, which reflect the high feed and permeate flow rates and the flow turbulence. This further resulted in a significant decrease in the temperature polarization effect due to the decrease in the thermal boundary layers' resistances.

### 4.3. Evaporation correction factor

The ratio between the evaporation rates of saline water to freshwater is empirically derived and used. The nomenclature for this ratio is $K_{sc}$ (evaporation correction factor) such that:

$$K_{sc} = E_{sal}/E_{fresh} \tag{25}$$

where $K_{sc}$ ($0 > K_{sc} > 1$) is the reduction in evaporation due to salinity, $E_{sal}$ is the rate of evaporation per unit area of saline water surface and $E_{fresh}$ is the rate of evaporation per unit area of freshwater surface. Studies involving primarily inland saline water bodies have reported this ratio. Bonython [13,14] used a thermally insulated evaporation pans over two summers to examine the effect of saline water with density varying from 1.07 to 1.245 $g/cm^3$. He reported the ratio of salt water evaporation to freshwater evaporation as a function of the density of the solution. The resulted data are used in the comparison of the data reported later.

Using the assumption of exponential relation between salinity and evaporation rate, the correlation can be in the initial form of:

$$K_{sc} = ae^{-Sab} + c \tag{26}$$

where $S$ is the water salinity and $a$, $b$ and $c$ are constants. Using values of $S$ and $K_{sc}$ that have been used practically by Pyramid Hill© salt company in Australia, $a$, $b$, and $c$ can be determined. The resulted correlation is as follows:

$$K_{sc} = 0.4e^{-0.04S\,(\%)} + 0.6 \tag{27}$$

Fig. 8a shows the improvement in the predicted mass flux after incorporating the correlation in the computer model. It can be seen that new corrected $J$ values have less deviation than the first theoretical values. This figure indicates that this deviation in the corrected values of the mass flux is between 10 and 14% greater than the experimental values for salinities from 0.1 to 20% whereas with lower concentration, it has less

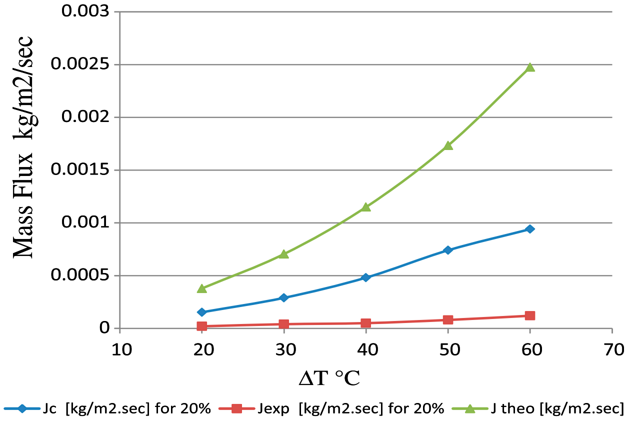

Fig. 8(a). The justified $J$ after applying the correction factor for water salinity of 20%.

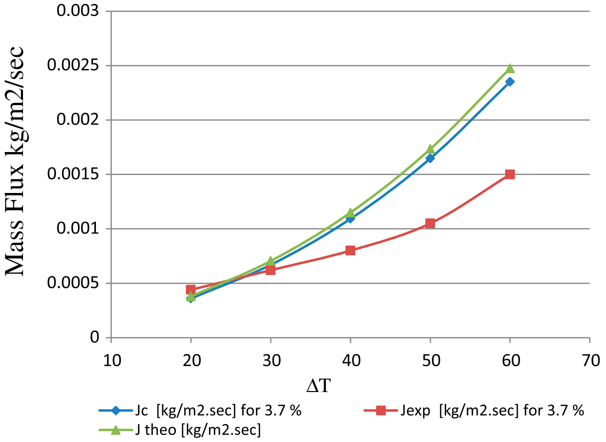

Fig. 8(b). The justified $J$ after applying the correction factor for water salinity of 3.7%.

effect as it is shown in Fig. 8b. In this figure, the applied correction achieves good agreement between the theoretical and experimental mass flux. Consequently, the modelling program can be modified using the correction factor to provide a reasonable predication for the performance of different DCMD modules.

The overestimation of $J$ at higher concentrations is due to the concentration effect on the mass flux which was initially not considered in the mathematical model. Although the correction factor was used to terminate the deviation, the theoretical values of $J$ still higher than that of experimental values except for lower concentrations.

### *4.4. Analysis of heat transfer*

The TPCs ($\lambda$) are presented in Fig. 7. The coefficients range from 0.27 to 0.32 for this study, indicating the higher effect of TPC on heat balance. The low feed velocity resulted in lower TPCs. The reasons were given above. On the other hand, the coefficients decreased with feed temperature decrease. The value of evaporation heat transfer rate changed from 200 to 6,000 W/m$^2$, whereas the thermal efficiency of the system improved from 7 to 28% when the temperature difference was increased from 20 to 60°.

### *4.5. Heat transfer rates*

The increase in $h_f$ is less significant compared with that due to feed velocity because of the dependence of heat of vaporization ($H_v$) on the temperature [12]. At a constant feed temperature, the heat transfers at feed side were higher for more concentrated solutions. This was related to lower permeation fluxes. In other words, with lower flux the decrease in membrane surface temperature was not considerable. The heat transfer components are shown in Figs. 9 and 10. Heat flux within membrane solid (sensible heat) increased from 5,000 to 18,000 W/m$^2$ with feed temperature increase, but decreased for higher concentration. Also, the latent heat transfer by mass flux which is considered a useful energy increased from 200 to 6,000 W/m$^2$, and this was in agreement with the above discussion. With a constant heat transfer coefficient for the permeate stream, it is observed that feed stream heat transfer in the membrane controlled the system heat transfer with its rate approximately 2–6 times higher than those of the vaporization heat transfer rate. The percentage of conduction loss through the membrane was 71–85%; it increased with feed concentration, but decreased with increasing temperature.

The increased concentration decreases the heat and mass transfer from the bulk feed side to the membrane surface due to the increase in solution viscosity and density which affects the heat transfer coefficient. The net effect is an increase in temperature gradient between the bulk feed phase and the membrane surface on feed side with solution concentration. The solution concentration has very less role in flux reduction as compared to the thermal polarization at low feed concentration, whereas the flux reduction due to concentration becomes important only at high feed

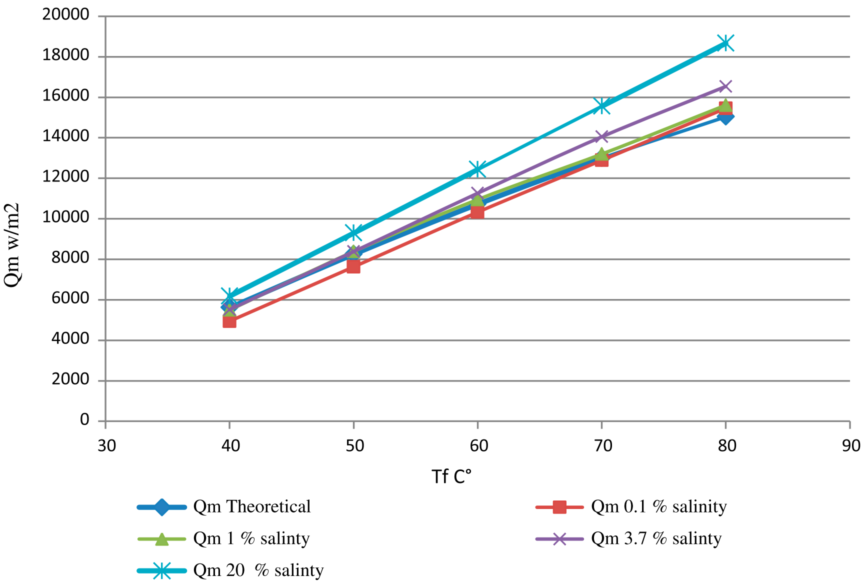

Fig. 9. The variation in heat transfer rates through the membrane solid material with feed temperature at different salinities.

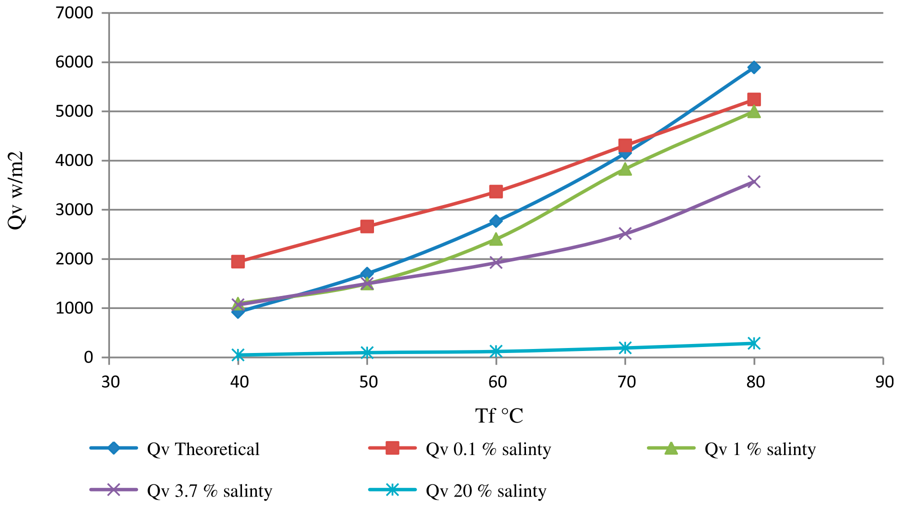

Fig. 10. Heat transfer rates by mass flux through the membrane.

concentration. The thermal polarization becomes worse at high solution concentrations, indicating a coupling of heat and mass transfer with the solution concentration.

### 4.6. Evaporation efficiency

Fig. 11 shows the effect of the temperature difference $\Delta T$, on the evaporation efficiency. Evaporation efficiency is defined as the ratio of the heat transferred by mass flux (latent heat) to the overall heat transferred through the membrane. The data shown in Fig. 10 represent, in addition to the evaporation efficiency, the mass transfer contribution to the overall heat transfer. This figure shows that the evaporation efficiency increases with feed temperature increase. Also, the mass flux contribution to the overall heat transfer through the membrane wall increases with the temperature difference increase since the permeate water vapour flux exhibited an exponential increase with the temperature increase as discussed before. Overall, the EE values which are ranging between 10 and 30% in Fig. 11 are low, and they are lower at lower operating temperatures. Therefore, if working at lower temperatures is required, probably only the availability of cheap energy such as solar energy could make this process economically feasible.

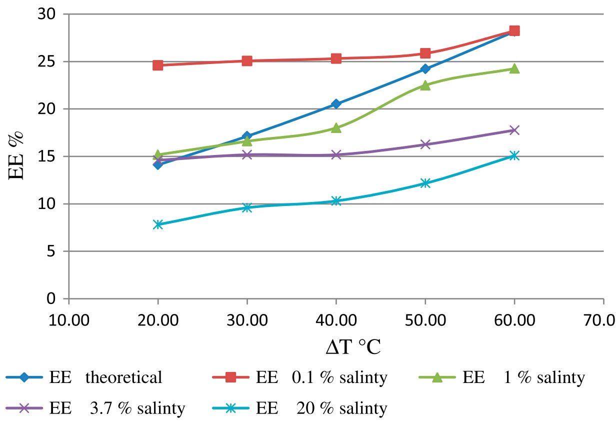

Fig. 11. Effect of temperature difference on evaporation efficiency with different salinities.

## 5. Conclusions

The effect of salinities and feed inlet temperature on heat and mass transfer in DCMD was investigated theoretically and experimentally. It was concluded that the membrane mass flux increases by increasing the temperature difference between feed and permeate flow. Also, the TPC increases by increasing the feed temperature. The dependence of membrane mass flux on temperature polarization is not linear and increases exponentially at TPC greater than 0.29. The TPC increased from 0.27 to 0.32, value of evaporation heat transfer rate changed from 200 to 6,000 $W/m^2$, whereas the thermal efficiency of the system improved from 7 to 28% when the temperature difference was increased from 20 to 60˚. At various feed inlet temperatures, the mass transfer can be better explained by using Knudsen and molecular diffusion transition model.

The value of MD coefficient ($C_m$) obtained in this study was 0.001 kg/m$^2$/s/Pa which is less than that reported in the literature. This is due to low water flow at both sides of the membrane. Also, the mass transfer contribution to the heat transfer was significant only in the membrane pores, while it was insignificant in both feed and permeates sides.

Finally, the modelling program can be modified and improved by using the correction factor to provide a reasonable predication for the performance of different DCMD modules.

## Nomenclature

$J$ — total mass flux of the membrane kg/m$^2$ h
$C_m$ — membrane mass flux coefficient kg/m$^2$ P$_a$ h
$C_{ap}$ — specific heat coefficient J/kg K
$P_1$ — vapour pressure at feed membrane surface (P$_a$)
$P_2$ — vapour pressure at permeate membrane surface (P$_a$)
$\tau$ — membrane tortuosity
$\Delta$ — membrane thickness (m)
$d$ — membrane pore diameter (m)
$\varepsilon$ — membrane piorosity
$R$ — gas constant (J/kg K)
$P_a$ — entrapped air pressure (P$_a$)
$M$ — molecular weight (kg/mol)
$T_f$ — bulk feed side temperature (K)
$T_p$ — bulk permeate side temperature (K)
$h_f$ — heat transfer coefficient at feed side (W/m$^2$K)
$h_p$ — heat transfer coefficient at permeate side (W/m$^2$K)
$h_m$ — heat transfer coefficient of the membrane (W/m$^2$K)

## References

[1] M.A. Hanjra, M.E. Qureshi, Global water crisis and future food security in an era of climate change, Food Policy 35 (2010) 365–377.
[2] P. Ranjan, S. Kazama, M. Sawamoto, A. Sana, Global scale evaluation of coastal fresh groundwater resources, Ocean Coast. Manage. 52 (2009) 197–206.
[3] M.R. Qtaishat, F. Banat, Desalination by solar powered membrane distillation systems, Desalination 308 (2013) 186–197.
[4] L. Mee, Between the Devil and the Deep Blue Sea: The coastal zone in an Era of globalisation, Estuarine Coastal Shelf Sci. 96 (2012) 1–8.
[5] M. Khayet, Membranes and theoretical modeling of membrane distillation: A review, Adv. Colloid Interface Sci. 164 (2011) 56–88.
[6] H. Susanto, Towards practical implementations of membrane distillation, Chem. Eng. Process. 50 (2011) 139–150.
[7] M.S. El-Bourawi, Z. Ding, R. Ma, M. Khayet, A framework for better understanding membrane distillation separation process, J. Membr. Sci. 285 (2006) 4–29.
[8] D. Winter, J. Koschikowski, M. Wieghaus, Desalination using membrane distillation: Experimental studies on full scale spiral wound modules, J. Membr. Sci. 375 (2011) 104–112.
[9] A. Alkhudhiri, N. Darwish, N. Hilal, Membrane distillation: A comprehensive review, Desalination 287 (2012) 2–18.
[10] S. Srisurichan, R. Jiraratananon, A.G. Fane, Mass transfer mechanisms and transport resistances in direct contact membrane distillation process, J. Membr. Sci. 277 (2006) 186–194.
[11] F.P. Incropera, P.I. Frank, Fundamentals of Heat and Mass Transfer, Wiley, New York, NY, 2002.
[12] M. Qtaishat, T. Matsuura, B. Kruczek, M. Khayet, Heat and mass transfer analysis in direct contact membrane distillation, Desalination 219 (2008) 272–292.
[13] Bonython, C. Warren & UNESCO, The Influence of Salinity upon the Rate of Natural Evaporation, UNESCO, Paris, 1958.
[14] Bonython, C. Warren & Northern Ohio Geological Society & Symposium on Salt (2nd: 1965: Cleveland), Factors Determining the Rate of Solar Evaporation in the Production of Salt, Reprinted from: Second Symposium on Salt, Cleveland, OH, 1966.

## Appendix A: Sample of the computer model results

| For 3.7% water salinity | $\Delta T$ = 40−20 = 20°C | $\Delta T$ = 50−20 = 30°C | $\Delta T$ = 60−20 = 40°C | $\Delta T$ = 70−20 = 50°C | $\Delta T$ = 80−20 = 60°C |
|---|---|---|---|---|---|
| Vmf (m/s) | 0.075 | 0.075 | 0.075 | 0.075 | 0.075 |
| Ref (DL) | 451.6824635 | 537.037403 | 625.9795127 | 719.3270003 | 813.8408831 |
| $h_f$ (w/m$^2$ k) | 907.1075953 | 918.7292894 | 927.339848 | 933.8611949 | 939.0185293 |
| Vmp (m/s) | 0.1136364 | 0.1136364 | 0.1136364 | 0.1136364 | 0.1136364 |
| Rep (DL) | 448.6522451 | 448.6522451 | 448.6522451 | 448.6522451 | 448.6522451 |
| $h_p$ (w/m$^2$ k) | 1,006.336491 | 1,006.336491 | 1,006.336491 | 1,006.336491 | 1,006.336491 |
| Path length (m) | 0.0000033 | 0.0000025 | 0.0000019 | 0.0000015 | 0.0000012 |
| Knudsen number (DL) | 14.7963019 | 11.3900205 | 8.8461152 | 6.9322596 | 5.4806545 |
| $H_v$ (J/kg) | 2,430,500 | 2,418,500 | 2,406,500 | 2,394,000 | 2,381,500 |
| $U$ (w/m$^2$ k) | 329.1273444 | 329.3346862 | 329.7239746 | 331.2586671 | 335.1440401 |
| $q_t$ (w/m$^2$) | 6,582.546888 | 9,880.040586 | 13,188.95898 | 16,562.93335 | 20,108.6424 |
| EE (DL) | 0.162463 | 0.1517676 | 0.1459706 | 0.1517666 | 0.1776475 |
| TPC (DL) | 0.3101134 | 0.3142714 | 0.3167932 | 0.3161078 | 0.3100574 |
| $T_1$ (k) | 305.743367 | 312.2459719 | 318.7776423 | 325.2640308 | 331.5854679 |
| $T_2$ (k) | 299.5410993 | 302.81783 | 306.1059135 | 309.4586433 | 312.9820265 |
| $P_1$ (Pa) | 4,949.492977 | 7,083.141488 | 9,980.280114 | 13,808.86645 | 18,682.94727 |
| $P_2$ (Pa) | 3,456.80128 | 4,187.602948 | 5,051.772293 | 6,087.482696 | 7,368.350862 |
| $C_m$ (kg/m$^2$ pa s) | 2.495E−07 | 2.475E−07 | 2.455E−07 | 2.436E−07 | 2.418E−07 |
| $J$ (kg/m$^2$ s) | 0.00044 | 0.00062 | 0.0008 | 0.00105 | 0.0015 |